

Case Studies of Aerosol Retrievals over the Ocean from Multiangle, Multispectral Photopolarimetric Remote Sensing Data

JACEK CHOWDHARY AND BRIAN CAIRNS

Department of Applied Physics and Applied Mathematics, Columbia University, New York, New York

LARRY D. TRAVIS

NASA Goddard Institute for Space Studies, New York, New York

(Manuscript received 8 January 2001, in final form 26 July 2001)

ABSTRACT

To evaluate the global effects of aerosols on the direct radiative balance, tropospheric chemistry, and cloud properties of the earth's atmosphere requires high-precision remote sensing that is sensitive to the aerosol optical thickness, size distribution, refractive index, and number density. This study uses the multiangle 0.41-, 0.55-, 0.865-, and 2.25- μm channel data from the airborne Research Scanning Polarimeter to retrieve aerosol properties over the Pacific Ocean. It is shown that such photopolarimetric data are highly sensitive to the size distribution and refractive index of aerosol particles, which reduces the nonuniqueness in aerosol retrievals using such data as compared with less comprehensive datasets. Moreover, it is found that polarized reflectances obtained at the shorter wavelengths (0.41 and 0.55 μm) are significantly less sensitive to the contribution of the ocean's upwelling light than total reflectance measurements, providing a natural tool for the separation between the estimation of oceanic and atmospheric scattering properties.

1. Introduction

Aerosols are believed to have a significant impact on the radiative balance and chemistry of the troposphere. Model computations show that the former effect, which includes the so-called indirect aerosol effect or aerosol-induced changes in the reflection properties of clouds, can be comparable in magnitude but opposite in sign to that of anthropogenic greenhouse gases (Houghton et al. 1996). They also suggest that aerosol-induced heterogeneous reactions reduce the global average NO_x burden by half (Dentener and Crutzen 1993). Reliable evaluation of both of these effects and of aerosol transport models used to provide present and future aerosol climatologies, requires precise global measurements of the aerosol optical thickness, chemical composition, size distribution, and number density. Thus far, the only operational aerosol satellite product available has been the optical thickness retrieved over the ocean using channel-1 radiances from the Advanced Very High Resolution Radiometer (AVHRR; Stowe and Ignatov 1997). The accuracy of this product is limited by the use of a single-wavelength (λ), single-viewing angle (θ) algorithm, which necessitates making prior assumptions about all

the other parameters of the atmosphere-ocean system. Although it is possible to improve the accuracy of the optical thickness retrievals from AVHRR measurements and also to determine the aerosol Ångström exponent by including channel-2 radiances (Higurashi and Nakajima 1999) there are still many untested prior assumptions required in the retrieval process (Mishchenko et al. 1999).

Aerosols also represent a problem for the spaceborne remote sensing of ocean color by instruments such as the Coastal Zone Color Scanner, the Sea-viewing Wide Field-of-view Sensor, and the Ocean Color and Temperature Scanner. Ocean color monitoring uses estimates of ocean water-leaving radiances to derive information on phytoplankton concentrations. These radiances become largest in the visible part of the spectrum where the absorption by pure ocean water is least, but still represent less than 20% of the total radiance observed from space. To distinguish the ocean signal from atmospheric scattering, it is common to estimate the latter contributions from near-infrared ($\geq 0.7 \mu\text{m}$) radiances, which are least sensitive to water-leaving radiances (Gordon 1997). Obviously any errors in the atmospheric correction (the estimation of aerosol composition, optical depth, and size distribution) will be propagated into errors in ocean color and chlorophyll-like pigment concentration estimates. Moreover, any uncertainties in the separation of the observed radiances into the contri-

Corresponding author address: Dr. Brian Cairns, NASA GISS, 2880 Broadway, New York, NY 10025.
E-mail: bc25@columbia.edu

TABLE 1. Comparison of capabilities of five instruments for tropospheric aerosol remote sensing. I = intensity, P = polarization, 3 for P.

Instrument	Number of bands	Spectral range (μm)	Number of view angles	Type of data
AVHRR	2	0.650–0.850	1	I
MODIS	7	0.470–2.130	1	I
MISR	4	0.443–0.865	9	I
POLDER	4	0.443–0.865	<14	I, P
EOSP	9	0.410–2.250	152	I, P

butions from ocean and atmosphere will impose limits on the potential of shorter wavelength measurements to constrain aerosol retrievals.

An array of new satellite instruments has recently been deployed to provide more complete observations of the earth's land, ocean, and atmosphere. We note in particular the moderate resolution imaging spectrometer (MODIS; King et al. 1992), the multiangle imaging spectroradiometer (MISR; Diner et al. 1991), and the Polarization and Directionality of the Earth's Reflectance (POLDER) instrument (Goloub et al. 1999). These instruments monitor the intensity (i.e., Stokes parameter I) of sunlight reflected by terrestrial systems in more wavelengths (MODIS, MISR, POLDER) and from more viewing angles (MISR, POLDER) than the AVHRR instrument (Table 1), and in addition measure the linearly polarized component (i.e., Stokes parameters Q and U) of reflected radiation (POLDER). The improvements that these instruments will make should, however, be contrasted with the accuracy requirement for climatologically useful aerosol retrievals (Hansen et al. 1995). Although the increased spectral range available from these instruments enhances their capability to retrieve particle size distributions, simulations performed for MODIS-type retrievals have already demonstrated significant difficulties in distinguishing between monomodal and multimodal size distributions (Tanré et al. 1996). The inclusion of measurements of the angular variation in the reflected radiation field in remote sensing allows for a higher sensitivity to aerosol type, but sensitivity analyses for MISR-type retrievals (Mishchenko and Travis 1997a) show that such data may still lead to ambiguous solutions for the aerosol refractive index and effective radius, both of which vary with relative humidity.

The fact that these intensity-only approaches to the retrieval of aerosol properties have such serious limitations suggests that an alternative measurement approach is necessary. Reflected solar radiation is, in general, polarized and contains embedded information about the intrinsic nature of aerosol particles as well as the underlying surface. Most of the detailed physical information about aerosols (e.g., particle size distribution, composition based on the spectral signature of refractive indices, particle shape) is only readily available through the measurement and analysis of the spectral

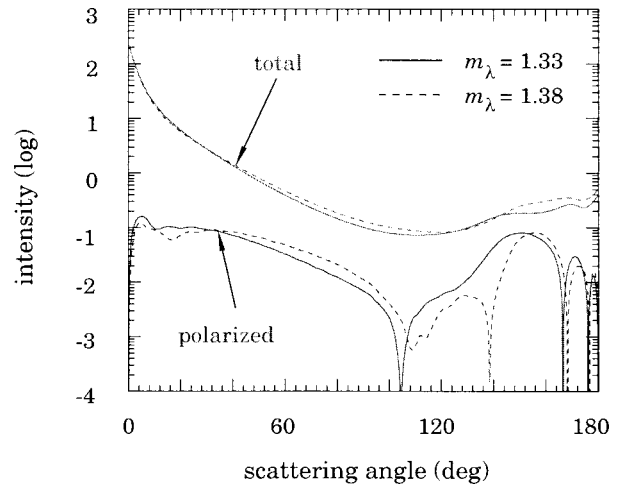


FIG. 1. The total and polarized intensity of light scattered once at the wavelength $\lambda = 0.865 \mu\text{m}$ as a function of scattering angle by a particle with effective radius $r_{\text{eff}} = 1.0 \mu\text{m}$ and refractive index $m_{\lambda} = 1.33$ (solid lines) and 1.38 (dashed lines).

and angular polarization signature of the reflected radiation. The principal reason for the greater effectiveness of remote sensing by means of polarization measurements is the significantly greater sensitivity of polarization features to particle size, shape, and refractive index as a function of scattering angle and wavelength, than is the case for intensity measurements. When multiple scattering effects are included, the strength of intensity features is considerably diminished, while the single-scattering information is largely retained in the polarization measurements.

Not only do polarimetric measurements contain more information about aerosols than intensity measurements, but there are also instrumental design and calibration advantages to making polarization measurements. For example, it is possible, with a well designed polarimetric instrument, to achieve absolute polarimetric accuracy of 0.2% on an operational basis. This high polarimetric accuracy ensures that any error in the absolute calibration of the polarized reflectance measurements used in this paper is almost identical to, and in the same sense as, the absolute calibration of the reflectance measurements.

An example of the sensitivity of polarization features to refractive index is given in Fig. 1, which shows the total and polarized intensity as a function of scattering angle for light with a wavelength of $0.865 \mu\text{m}$ scattered once by particles with identical size distributions (effective radius of $1.0 \mu\text{m}$) but different refractive indices m_{λ} . Another example, based on actual POLDER data, for a case where there is significant multiple scattering is given by Bréon and Goloub (1998) who compare the sensitivity of polarized and total reflectances to cloud droplet effective radii. In spite of the potential of polarimetric measurements to retrieve aerosol properties, comparisons with ground-based sun photometer mea-

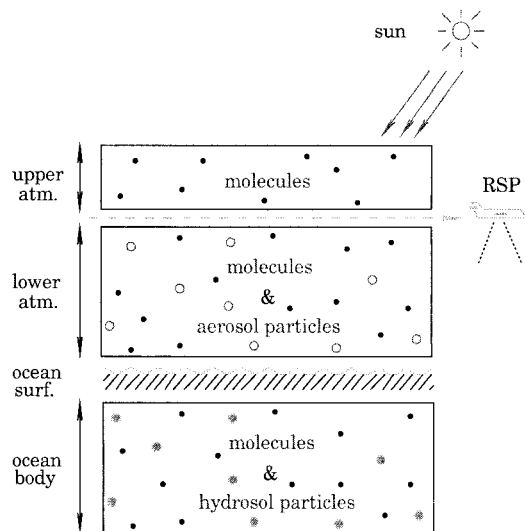


FIG. 2. The atmosphere-ocean system used for simulating RSP datasets obtained from aircraft over the ocean.

measurements still reveal systematic errors in POLDER-derived Angström exponents (Goloub et al. 1999). Recent analyses suggest that the simultaneous occurrence of small and large aerosol particles may be responsible for some of the discrepancies found in these retrievals, which currently assume monomodal size distributions (Deuzé et al. 2000). Based on in situ sampling measurements and our understanding of the processes of aerosol formation, removal, and transport (Jaenicke 1993), such bimodal aerosol mixtures are expected to be ubiquitous, but the resolution of the two modes in the aerosol size distribution has proved difficult with the relatively small spectral range (0.67 and 0.865 μm) of POLDER observations currently used.

In this paper, we discuss aerosol retrievals over the ocean using data collected with the Research Scanning Polarimeter (RSP) instrument (Cairns et al. 1999), an airborne instrument that is functionally similar to the Earth Observing Scanning Polarimeter (EOSP; Travis 1993). The RSP instrument was designed to provide high-precision, multiangle measurements of polarization and intensity in a wide spectral range from the visible to the short-wave infrared (Table 1). This allows us to build on the analyses and results of the MODIS, MISR, and POLDER teams, since the RSP instrument provides measurements that are similar to, and in many respects more comprehensive than, all three satellite instruments. In a recent paper, we demonstrated by applying inversion methods to different subsets of RSP data how the range of available measurements in a dataset affects the nonuniqueness problem faced in the parameter estimation problem, which is the remote sensing of aerosols (Chowdhary et al. 2001). Our results, based on employing just two narrowband channels (0.865 and 2.25 μm), demonstrated the superiority of using multiangle intensity and polarization measure-

ments over approaches that use more limited measurement sets. In this paper we explore the use of observations at shorter wavelengths (0.41 and 0.55 μm) and examine the water-leaving contribution to the observed intensity and polarization. This analysis is designed to determine whether the signals from the ocean and from aerosols at these shorter wavelengths can be better separated by using both intensity and polarization measurements. We also examine, using different subsets of RSP data, how the completeness of the available dataset affects aerosol retrievals and the consequences of any errors in these retrievals for the estimation of ocean color.

2. Instrument design and performance

The properties of the RSP instrument and measurements that form the basis for the analyses in the next section are discussed in the following. The 14-mrad instantaneous fields of view (IFOV) of the six bore-sighted RSP telescopes are continuously scanned by a polarization-neutral two-mirror system that allows 152 viewing-angle samples to be acquired over a 120° swath ($\pm 60^\circ$ from nadir). The desired polarization-insensitive scanning function of the RSP is achieved by the use of a two-mirror system with the mirrors oriented such that any polarization introduced at the first reflection is compensated for by the second reflection. The refractive telescopes are paired, with each pair making measurements in three spectral bands. One telescope in each pair makes simultaneous measurements of the linear polarization components of the intensity in orthogonal planes at 0° and 90° to the meridional plane of the instrument (using Wollaston prisms to spatially separate the orthogonal polarizations onto a pair of detectors) while the other telescope in a pair simultaneously measures equivalent intensities in orthogonal planes at 45° and 135°. These measurements in each instantaneous field of view in a scan provide the simultaneous determination of the Stokes parameters I , Q , and U in all nine spectral bands with a wide dynamic range (14-bit digitalization) and high signal-to-noise ratio (2000 at a Lambertian equivalent reflectance of 0.3). This approach ensures that the polarization signal is not contaminated by scene intensity variations during the course of the polarization measurements, which could create “false” or “scene” polarization.

The instrument has nine spectral channels that are divided into two groups based on the type of detector used: visible-near-infrared bands using UV-enhanced silicon photodiodes at wavelengths of 410 (30), 470 (20), 550 (20), 670 (20), 865 (20), and 960 (20) nm, and short-wave infrared bands using HgCdTe photodiodes (cooled to 163 K) at wavelengths of 1590 (60), 1880 (90), and 2250 (120) nm. Dichroic beam splitters are used for spectral selection, while interference filters define the spectral bandpasses of each band. The paranthetic figures are the full width at half maximum band-

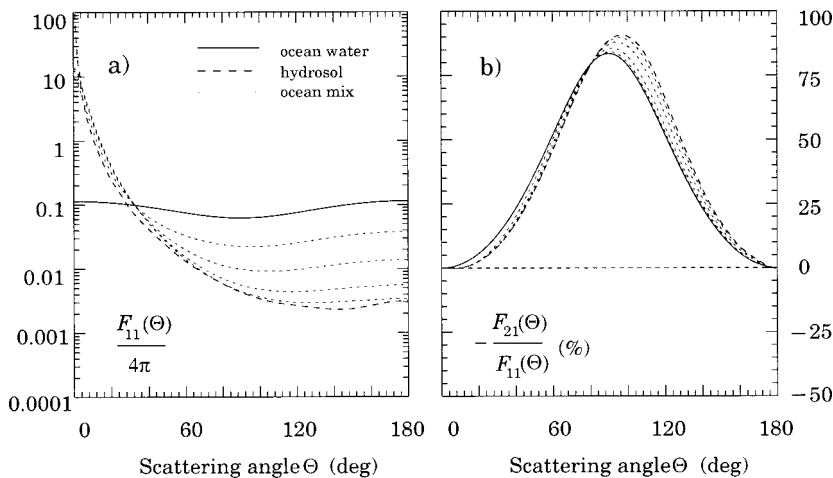


FIG. 3. The phase functions F_{11} normalized by 4π (left) and the linear polarization ratios $-F_{21}/F_{11}$ (right) used for the underwater light computations as a function of the scattering angle. The hydrosol in the left and right panel stands for the average values used by Mobley et al. (1993) and the hydrosol particles specified in the text, respectively. The ocean mix curves are shown for chlorophyll-like pigment concentrations $[C] = 1.000, 0.100, 0.010,$ and 0.001 mg m^{-3} .

widths of the spectral bands. These spectral bands sample the spectrum of reflected solar radiation over most of the radiatively significant range, with measurements under typical clear-sky conditions ranging from significant Rayleigh scattering (410 nm) to single scattering by aerosol (2250 nm) within a single dataset.

The expected radiometric uncertainty is 3.5% using a reflectance-based mountaintop calibration. The uncertainty in degree of linear polarization measurements is 0.2% (Cairns et al. 1999), based on instrument characterization and pre- and postflight relative calibrations of the detectors for a particular spectral band within a given telescope. Since the polarimetric and radiometric calibration paths are independent this implies that the polarized reflectance measurements have an uncertainty that is almost identical to the radiometric uncertainty (i.e., 3.51%).

3. Model description and data simulations

We adopt for our analyses the same simple atmosphere–ocean model system used in Chowdhary et al. (2001; see Fig. 2). Aerosol particles are homogeneously mixed with molecules below the aircraft and are generally assumed to have either a monomodal (accumulation) or a bimodal (accumulation and coarse mode) lognormal size distribution (cf. Nakajima et al. 1996). Trimodal (and higher number mode) solutions are also possible and the retrievals presented below are therefore by no means unique. However, a bimodal solution is the most parsimonious solution that is consistent with both the prior information from in situ sampling measurements and the remote sensing data used in this study. Following Hansen and Travis (1974), we use parameters that can be retrieved from remote sensing data to char-

acterize each aerosol mode, that is, the effective radius (r_{eff}) and effective variance (v_{eff}) of its size distribution, its refractive index (m_{λ}) as a function of wavelength, and its optical thickness (τ_{λ}) as a function of wavelength. In addition, we derive from these optical parameters the column number density of particles (N) for each aerosol component (Mishchenko et al. 1997b), a physical quantity of interest to the evaluation of the indirect aerosol effect. When retrieving the refractive index we require its real part to be decreasing as the wavelength increases in the near-infrared part of the spectrum, and to remain constant in the visible part of the spectrum. Such spectral behavior of (m_{λ}) is consistent with trends found in laboratory and in situ measurements of aerosol properties (e.g., d’Almeida et al. 1991), and facilitates the inversion process by reducing the size of the aerosol parameter space. In those cases where the absorption optical depth of aerosols is small, that is, low aerosol optical depths and/or single-scatter albedo close to unity, reflectance measurements over the ocean are not very sensitive to absorption. Also, scattering matrices of aerosol particles are not very sensitive to the imaginary part of refractive index except for strongly absorbing materials. For simplicity we therefore set the imaginary part of the refractive index to zero; that is, we ignore aerosol absorption. This indicates that there is a nonuniqueness issue in the retrieval of aerosol single-scatter albedo from reflectance and polarized reflectance measurements for low aerosol optical depths (Mishchenko and Travis 1997b), unless sun glint measurements are included in the analysis. The single-scattering properties of aerosol particles are obtained using the Mie theory, that is, the implicit assumption here is that the particles are spherical and homogeneously mixed. If the sphericity assumption is not true,

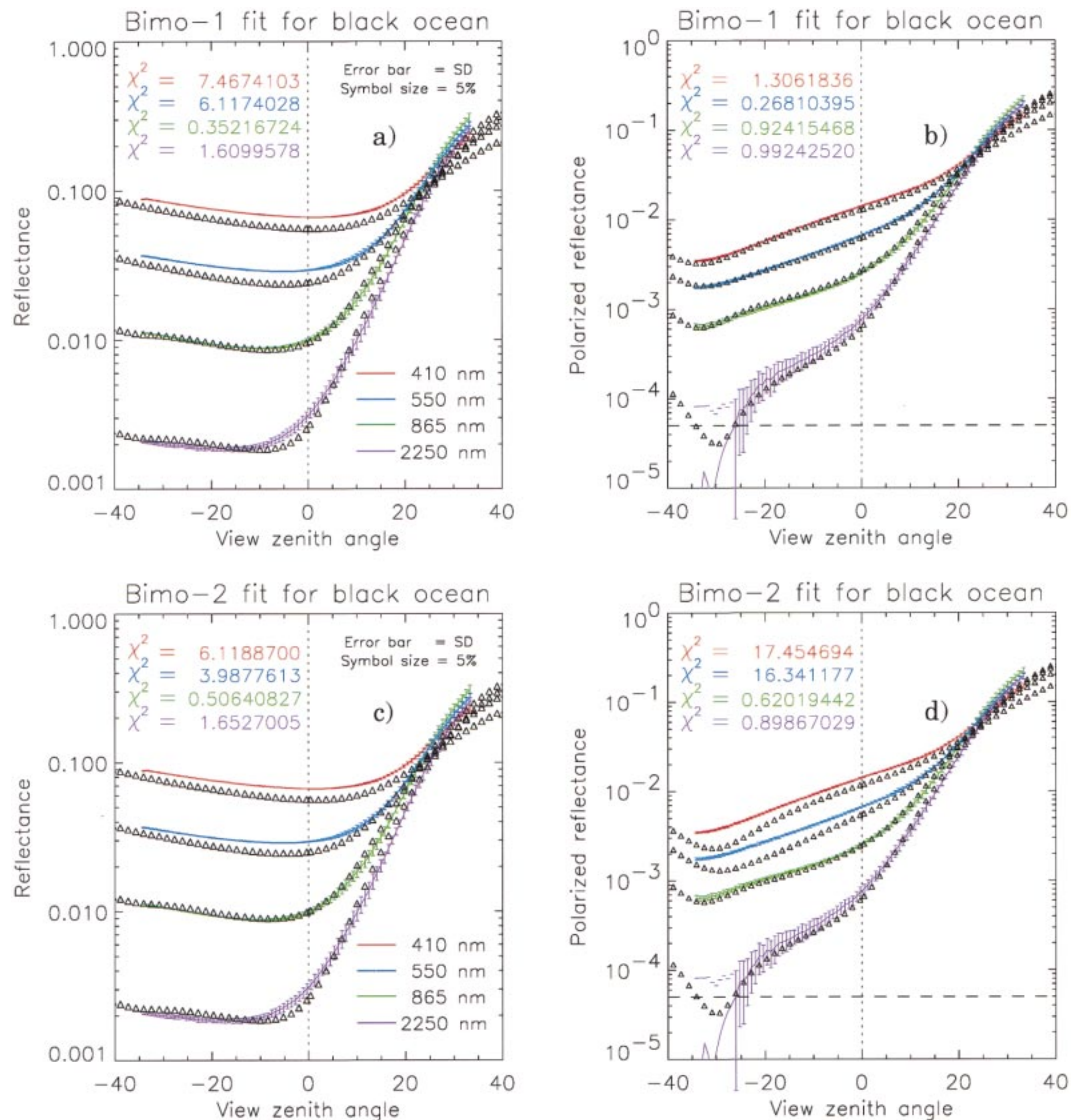


FIG. 4. (a) The fit (triangles) to the mean RSP reflectance data (lines) for $\lambda = 0.410, 0.550, 0.865,$ and $2.250 \mu\text{m}$ using the accumulation and coarse mode components of the bimo-1 aerosol model listed in Table 2 and assuming a black ocean body. Error bars denote the std dev of the RSP data, and the size of the triangles represents a 5% uncertainty in the results of our simulations. The goodness of the fit is given for each wavelength by the normalized chi-square value in the upper left corner. (b) Same as in (a), but for polarized reflectances. (c) Same as in (a), but for the bimo-2 aerosol model listed in Table 2. (d) Same as in (b), but for the bimo-2 aerosol model listed in Table 2.

then it will not be possible to achieve a satisfactory fit to the polarization measurements (Mishchenko et al. 1997a). In such a case (e.g., coarse mode consists of dust particles) we would then use computations of light scattering by shape distributions of polydisperse spheroids to represent nonspherical particles. As regards the homogeneity assumption, in all the extant data that we have analyzed, Mie theory calculations have provided excellent fits. Thus, it appears that the retrieved refractive indices are at least representative of an effective medium approximation (Chylek et al. 2000).

Gaseous absorption is assumed to occur above the scattering atmosphere, in the stratosphere, and is simply

modeled as an attenuation of the direct beam of the sun. This assumption is suitable for absorption by ozone in the Chappuis band, and we use for the latter absorption an ozone amount of 272 Dobson units, which is consistent with both the Total Ozone Mapping Spectrophotometer and multifilter rotating shadowband radiometer (MFRSR) measurements. Our assumption for gaseous absorption is probably less realistic for NO_2 ; however, the modeled amount (5 ± 1.5 ppb from MFRSR measurements; Alexandrov et al. 2002) is quite plausible given our current understanding of atmospheric NO_2 concentrations and distributions (Shaw 1976; Noxon 1978; Pujadas et al. 2000). It should be noted that the

TABLE 2. Aerosol size parameters, refractive indices, optical thicknesses, and column number densities retrieved from RSP data subsets.

Aerosol	r_{eff} (μm)	v_{eff}	m_{2550}	m_{550}	τ_{550}	N (m^{-2})
Bimo-1	1.0	1.0	1.40	1.42	0.022	2.2×10^{10}
	.25	.15	1.29	1.33	0.126	6.2×10^{11}
Bimo-2	1.0	1.0	1.40	1.42	0.022	2.2×10^{10}
	.25	.15	1.34	1.40	0.121	4.5×10^{11}
Bimo-3	0.8	0.3	1.35	1.37	0.024	9.4×10^9
	.30	.20	1.33	1.35	0.139	4.0×10^{11}
Mono-1	0.4	1.0	1.29	1.33	0.163	1.4×10^{12}
Mono-2	0.4	1.0	1.35	1.39	0.118	9.0×10^{11}
Mono-3	0.3	0.3	1.31	1.35	0.169	6.5×10^{11}

effects of gaseous absorption are corrected for in the RSP data, rather than being included in the model. The model comparisons with RSP data presented below are therefore for a purely scattering atmosphere. The molecular optical thickness that we use for the scattering atmosphere is that given by Hansen and Travis (1974) with a scale height of 8 km, which defines the amount of Rayleigh scattering above and below the aircraft.

The reflection and transmission properties of the ocean surface are calculated using the geometrical optics approach with a wind-speed-dependent surface slope distribution (Cox and Munk 1954), and with surface shadowing effects (Sancer 1969) and scattering by oceanic foam (Koepke 1984) taken into account. When inverting visible remote sensing data obtained over ocean bodies, one commonly approximates the intensity of the upwelling underwater light by means of a Lambertian surface with an albedo empirically related to the chlorophyll-like pigment concentration $[C]$, in mg m^{-3} (Gordon and Morel 1983). Such approximations are valid for retrievals based on near-nadir single-viewing angles and photometric measurements. However, the sensitivity of RSP measurements to the bidirectional (Morel and Gentilli 1995) and especially polarized nature (Voss and Fry 1984) of underwater light scattering requires a more rigorous approach for both the simulation and inversion of multiangle polarimetric remote sensing data of atmosphere–ocean systems. As an ansatz toward solving these problems, we perform polarized radiative transfer computations for the underwater light using realistic bulk oceanic scattering properties, and we perform sensitivity studies for the dataset analyzed in the

TABLE 3. Specification for the bimo-S model, and the optical thicknesses retrieved from the RSP total reflectance dataset.

Aerosol	r^*	σ^{**}	m_{2550}	m_{865}	m_{550}	m_{410}	τ_{550}
Oceanic	0.30	2.00	1.31	1.35	1.35	1.36	0.048
Soluble	0.005	2.99	1.42	1.52	1.53	1.53	0.067

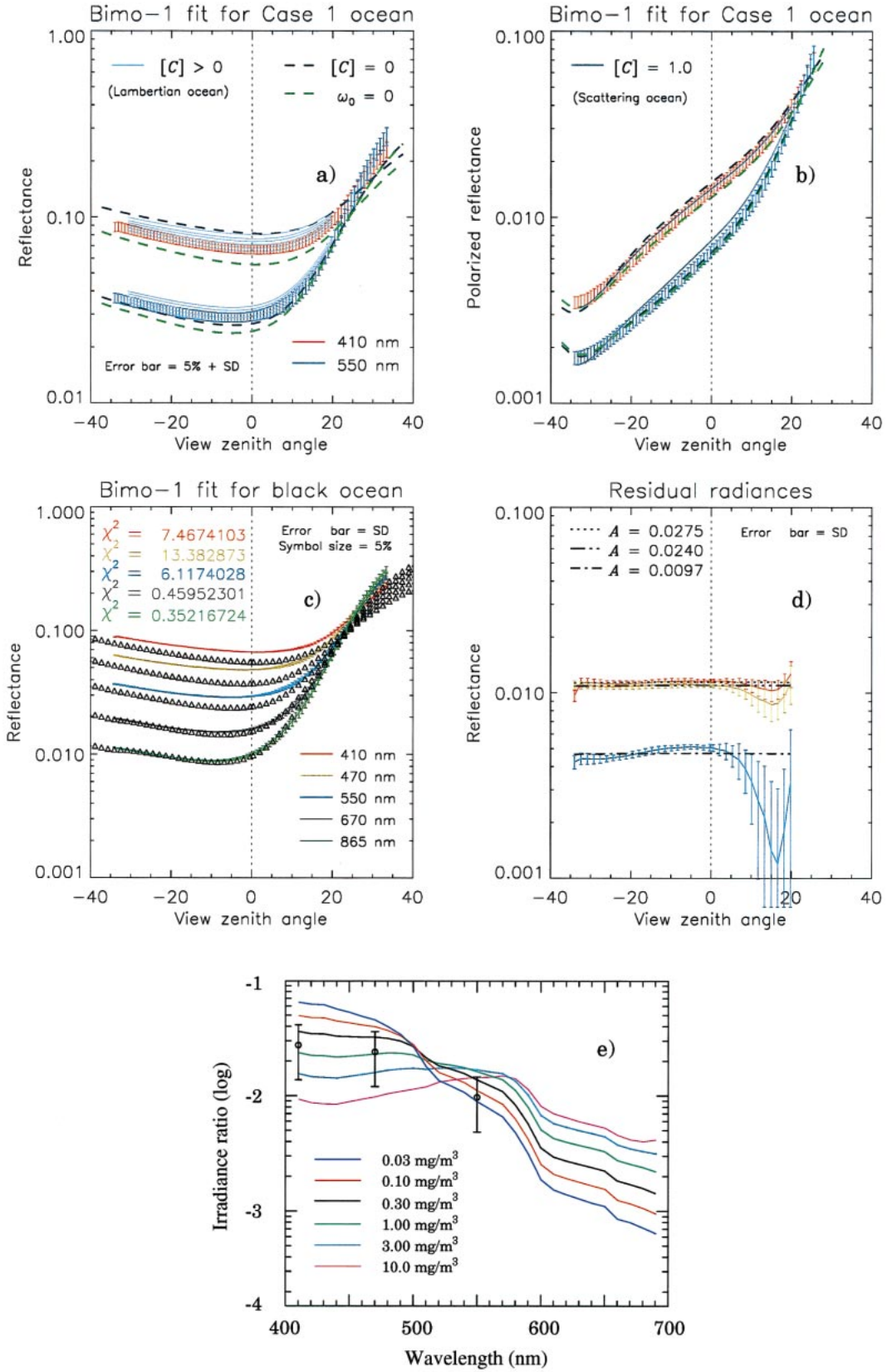
* Geometrical mean radius, μm .

** Geometrical standard deviation.

present work. We assume for this purpose that scattering in the ocean body is well approximated by a homogeneous mixture of clean oceanic water and hydrosol particles (Fig. 3). Scattering by clean oceanic water is modeled as Rayleigh scattering with a depolarization factor of 0.09 (Morel 1974), and with the scattering and absorption coefficients given by Hale and Querry (1973). The scattering by hydrosol particles is based on the application of Mie theory to particles with an inverse fourth-power law size distribution (Stramski and Kiefer 1991), lower bound of $0.001 \mu\text{m}$ and an upper bound of $3.0 \mu\text{m}$, and a refractive index of $1.10 - 0.0025i$ relative to that of water. This microphysical model gives rise to a phase function F_{11} (Fig. 3a) that closely resembles the averaged one given by Mobley et al. (1993) for all the hydrosol phase functions measured by Petzold (1977). Moreover, the linear polarization ratio $-F_{21}/F_{11}$ for these particles is similar to that found in laboratory measurements of phytoplankton (Volten et al. 1998), and is consistent with the rather small variation in the degree of linear polarization (Fig. 3b) found for bulk oceanic waters (e.g., Kadyshevich and Lyubovtseva 1973). The scattering and absorption coefficients for hydrosol scattering are taken from Morel (1988) for case 1 water, that is, oceanic surface waters for which the optical properties are dominated by phytoplankton and their by-products. Note that the dependence of these coefficients on (C) is consistent with that used for Lambertian ocean models. Finally, we adopt a bulk optical thickness of 10 for the ocean body.

Multiple scattering computations for the transport of light through this model atmosphere and ocean are performed using the fast doubling–adding method (De Haan et al. 1987; Chowdhary 1999). Different sets of Gaussian quadrature points are used for the skylight and underwater light directions to increase compu-

FIG. 5. (a) Error bars denote the sum of the std dev of the RSP data and a 5% uncertainty in model simulations, and are centered around the mean RSP data obtained at $\lambda = 0.410$ and $0.550 \mu\text{m}$. The green dashed lines show the corresponding bimo-1 aerosol model fits for a black ocean body (cf. Fig. 4a). The dark blue dashed lines are for including a molecular ocean, and the solid gray lines for using $[C] = 0.01, 0.05, 0.10, 0.40,$ and 1.00 mg m^{-3} for $\lambda = 410 \mu\text{m}$, and $[C] = 0.01, 0.05, 0.15, 0.40,$ and 1.00 mg m^{-3} for $\lambda = 550 \mu\text{m}$. (b) Same as in (a), but for polarized reflectances and taking $[C] = 1.00 \text{ mg m}^{-3}$ for the solid gray line. (c) Lines and error bars show the mean RSP reflectance data and their std dev, respectively, for $\lambda = 0.410, 0.470, 0.550, 0.670,$ and $0.865 \mu\text{m}$. The symbols denote the corresponding fits using the bimo-1 aerosol model of Table 2 and assuming a black ocean body as in Fig. 4a. (d) Lines are for the same wavelengths as in (c) but denote the difference between the RSP data and corresponding fits. The black broken lines show the reflectances of water-leaving radiances simulated for an ocean body that is approximated by a Lambertian surface with albedo A . (e) Irradiance ratios just below the ocean surface as a function of the wavelength and of $[C]$. The semiempirical curves are reproduced from Morel (1988). Inserted are the ocean albedos A from (d) with error bars denoting the uncertainty (50%) of Morel's (1988) equations for irradiance ratios.



tational efficiency, and we renormalize the ocean surface scattering properties to account for multiple reflections between ocean waves (isotropic renormalization) and to ensure conservation of energy (refraction peak renormalization). Although the numerical precision of our computations is better than five significant figures, uncertainties in the values, or spectral dependence of some of the parameters adopted for our atmosphere–ocean model lead to a lower confidence in the verisimilitude of our model when comparisons are being made to measurements of an actual ocean–atmosphere system. The principal sources of uncertainty are the surface fraction (Monahan and O’Muircheartaigh 1980) and spectral albedo (Frouin et al. 1996) of oceanic foam, the wind-directionality of the sun glint (Masuda 1988), and the scattering coefficient for hydrosols (Loisel and Morel 1998). We adopt an uncertainty of 5% for all our radiative transfer results to account for the potential of such errors in a priori assumptions. This uncertainty in the modeling of the system is also the reason that reflectance and polarized reflectance measurements are used in the following analyses, since it is easier to identify and diagnose modeling errors and uncertainties than in the (more accurate) degree of linear polarization.

4. Measurements and aerosol retrievals

a. Dataset

The data used for the present study were acquired off the coast of Santa Cruz Island, California, on 14 October 1999 with the RSP instrument mounted on an aircraft and the scanner oriented so that the plane of the scan is directed along the direction of the aircraft ground track. The scattering geometry for this dataset is given by the solar zenith angle $\theta_0 = 43^\circ$ and azimuth difference $\varphi - \varphi_0 = 3^\circ$ between the principal plane and RSP scan plane. The altitude (3000 m) and speed (50 m s^{-1}) of the aircraft were chosen such that successive nadir views were one IFOV apart and the same point at the ground was thus seen from multiple viewing angles, with the nadir pixel size being 42 m. Vignetting of the RSP scan by the skin of the aircraft made data at viewing angles larger than $\pm 40^\circ$ from nadir unavailable. In what follows, we actually show and analyze for each viewing angle θ the average of 40 consecutive same-viewing angle measurements. Our study focuses on measurements obtained at 0.41, 0.55, 0.865, and 2.25 μm . The longer two wavelengths are used to distinguish fine and coarse mode aerosol properties. Measurements obtained between these two wavelengths can be used to retrieve the spectral variation of refractive indices between 0.865 and 2.25 μm . The shorter two wavelengths are chosen to study the contributions of polarized and total reflectances that originate from underwater light scattering, and to assess the retrieval of aerosol properties from polarized visible light. These four spectral bands were

chosen as exemplars of the effects of atmospheric and ocean contributions and because they span the full spectral range of the RSP measurements. The bands at 0.47 and 0.67 μm were excluded from the analysis for simplicity and, in the case of the 0.67- μm band, because it can contain poorly characterized contributions from ocean body scattering (Toole et al. 2000). The remaining bands are not included in the analysis presented below because they are used for water vapor estimates (0.96 μm), cirrus cloud screening (1.88 μm), or were not functional (1.59 μm).

An MFRSR instrument was also used during the period of the RSP data collection to provide estimates of the aerosol optical depth, effective radius, effective variance, NO_2 and ozone column abundances, and the downwelling horizontal irradiance in five narrow spectral bands at 0.415, 0.501, 0.616, 0.672, and 0.869 μm (Alexandrov et al. 2002). The MFRSR was located 1 km inland near Oxnard, California, and airborne RSP measurements of the surface around the MFRSR were used to characterize the bidirectional reflectance distribution function of the surface so that the method of King and Herman (1979) could be used to estimate the single-scatter albedo of the aerosols. The measured aerosol optical depth at 0.55 μm was 0.14 (± 0.01) and the single-scatter albedo was estimated to be 0.95 (± 0.02) with negligible spectral variation. The absorption optical depth was therefore less than 0.01, which is why the neglect of absorption for the measurements presented below is considered reasonable.

b. Aerosol retrieval using the full set of RSP data

Our bimodal aerosol retrieval method incorporates the two steps followed in Chowdhary et al. (2001). The first step consists of using the 2.25- μm total and polarized reflectance measurements to estimate the coarse mode aerosol parameters under the assumption that the accumulation-mode aerosol optical thickness is (negligibly) small at this wavelength. The second step consists of using this estimate, together with the 0.865- μm total and polarized reflectance measurements, to estimate the parameters of the accumulation mode aerosol. In addition, we use in the present work the polarized reflectance measurements at 0.41 and 0.55 μm to verify, or refine, our aerosol estimates under the assumption that the ocean body is black (i.e., ignoring the contribution of water-leaving radiances). This process is iterated until it converges to a solution that is consistent with all of the above data. The rationale for using the visible polarized reflectances to constrain aerosol properties is discussed below, while in section 4c we address the contribution of water-leaving radiances.

The upper panels of Fig. 4 show data and the type of results that are obtained using this iterative estimate of aerosol properties. The left and right panel are for the total reflectance $\pi I(\mu_0 S)^{-1}$ and for the linearly polarized reflectance $\pi(Q^2 + U^2)^{1/2}(\mu_0 S)^{-1}$ as a function

of the view zenith angle, respectively. The view zenith angle θ is positive in the direction of the plane's flight (see Fig. 2), while $\mu_0 = \cos\theta_0$, and S is the extraterrestrial solar flux. Hence, the sharp increase in reflectance seen for positive viewing angles corresponds to the sun-glint profile. The mean and standard deviation of the RSP measurements are shown by the lines and error-bars, respectively. The symbols show model simulations for the estimated bimodal aerosol model (hereafter referred to as "bimo-1"; see Table 2). The goodness of the fit between measurements and simulations is given for each wavelength in the upper left corner of the panels by the normalized chi-square value (χ^2) defined as,

$$\chi^2 = \frac{1}{N} \sum_{i=1}^N \left[\frac{y_i - x_i}{S_i} \right]^2, \quad (1)$$

where N is the number of viewing angles analyzed, y_i is the simulated reflectance for viewing angle i , x_i is the average reflectance for viewing angle i , and S_i is the standard deviation of the combined error sources for viewing angle i ; that is,

$$S_i = \sqrt{(0.05y_i)^2 + (0.035x_i)^2 + \sigma_i^2}. \quad (2)$$

In Eq. (2), σ_i is the standard deviation of the measurements for viewing angle i ; that is, it is given by

$$\sigma_i = \sqrt{\frac{\sum_{j=1}^P (x_i^j - x_i)^2}{P - 1}}, \quad (3)$$

where P is the number of pixels used for each viewing angle analysis, and x_i^j is the reflectance of pixel j for viewing angle i . We used the standard deviation in the computation of the combined error rather than the standard error because pixel-to-pixel variations are caused not only by instrumental noise, but also by reflectance variations in the ocean surface and aircraft orientational changes. Equation (1) can therefore only be regarded as an ad hoc measure for the agreement between measurements and model calculations, with $\chi^2 \leq 2$ denoting acceptable to good results. Note also that angular variation of the reflected radiances is smooth, suggesting the existence of strong correlations between different viewing-angle measurements that should be accounted for in more rigorous statistical measures (Dubovik and King 2000). In what follows, we use only the angular range of $-35^\circ \leq \theta \leq 20^\circ$ to compute normalized chi-square values in order to avoid serious contamination by the sun glint, and we exclude polarized reflectance measurements smaller than 5×10^{-5} (horizontal dashed line) from this computation since they are at the digitization level of the RSP measurements.

There are a number of points to be noted for Figs. 4a and 4b. First, the sun-glint angular profile is quite sensitive to the wind speed W , which allowed us to constrain the wind speed to $4.5 (\pm 0.5) \text{ m s}^{-1}$. Second, the retrieved aerosol model has an optical thickness at

a reference wavelength of $0.55 \mu\text{m}$ of 0.148 (Table 2), which is in good agreement with the value of 0.14 measured that day at the same time at Oxnard, using an MFRSR. Third, the total reflectance measured at 0.41 and $0.55 \mu\text{m}$ is significantly larger than that which is simulated in these bands. The differences can be attributed to the neglect of water-leaving radiances in our computations (section 4c), although the variation of water-leaving radiances with the pigment concentration in the ocean makes it difficult to verify such results without complimentary knowledge on the biotic state of the ocean. The mixing of atmospheric and ocean contributions to the total upwelling reflectance observed at these shorter wavelengths may in fact pose a problem for the retrieval of accumulation-mode aerosol properties if one uses only photometric measurements. This is because the effective size parameter, $(2\pi r_{\text{eff}})/\lambda$, of sub-micron particles only becomes large enough at visible wavelengths for their single-scattering properties to be well differentiated from Rayleigh scattering (cf. Mishchenko and Travis 1997a). On the other hand, polarized reflectances measured in the visible part of the spectrum do provide useful constraints on the accumulation mode aerosol properties. Consider, for example, in Figs. 4c and 4d the results of an aerosol retrieval in which the polarized reflectance measurements at 0.41 and $0.55 \mu\text{m}$ are ignored. Note that a different bimodal aerosol model, hereafter referred to as "bimo-2," whose accumulation mode component differs from the one of bimo-1 by as much as 0.07 in refractive index (Table 2), is just as consistent with reflectance and polarized reflectance measurements at 0.865 and $2.25 \mu\text{m}$ as the bimo-1 model. It is only by including the 0.41- and $0.55\text{-}\mu\text{m}$ polarized reflectance that we start to observe significant discrepancies between measured and simulated polarized reflectances. We show in the next section that such discrepancies *cannot* be bridged by the inclusion of water-leaving radiances.

c. Contribution of water-leaving radiances

To evaluate the contribution of waterleaving radiances to the total and polarized reflectances observed by the RSP instrument, we perform here sensitivity studies for various ocean models. Consider first the case of a purely molecular scattering ocean in Figs. 5a and 5b (blue dashed lines). Note that the total reflectance computed at $0.41 \mu\text{m}$ is now larger than the corresponding RSP measurements, while the total reflectance computed at $0.55 \mu\text{m}$ is still less than the observed reflectance. This result is consistent with what one would expect for an ocean body with appreciable amounts of chlorophyll-like pigments, which absorb strongly in the blue but weakly in the green part of the visible spectrum (Morel 1988, and references therein). By subsequently increasing the amount of chlorophyll-like pigments in our ocean model we observe a convergence between our numerical calculations (solid gray lines) and the RSP

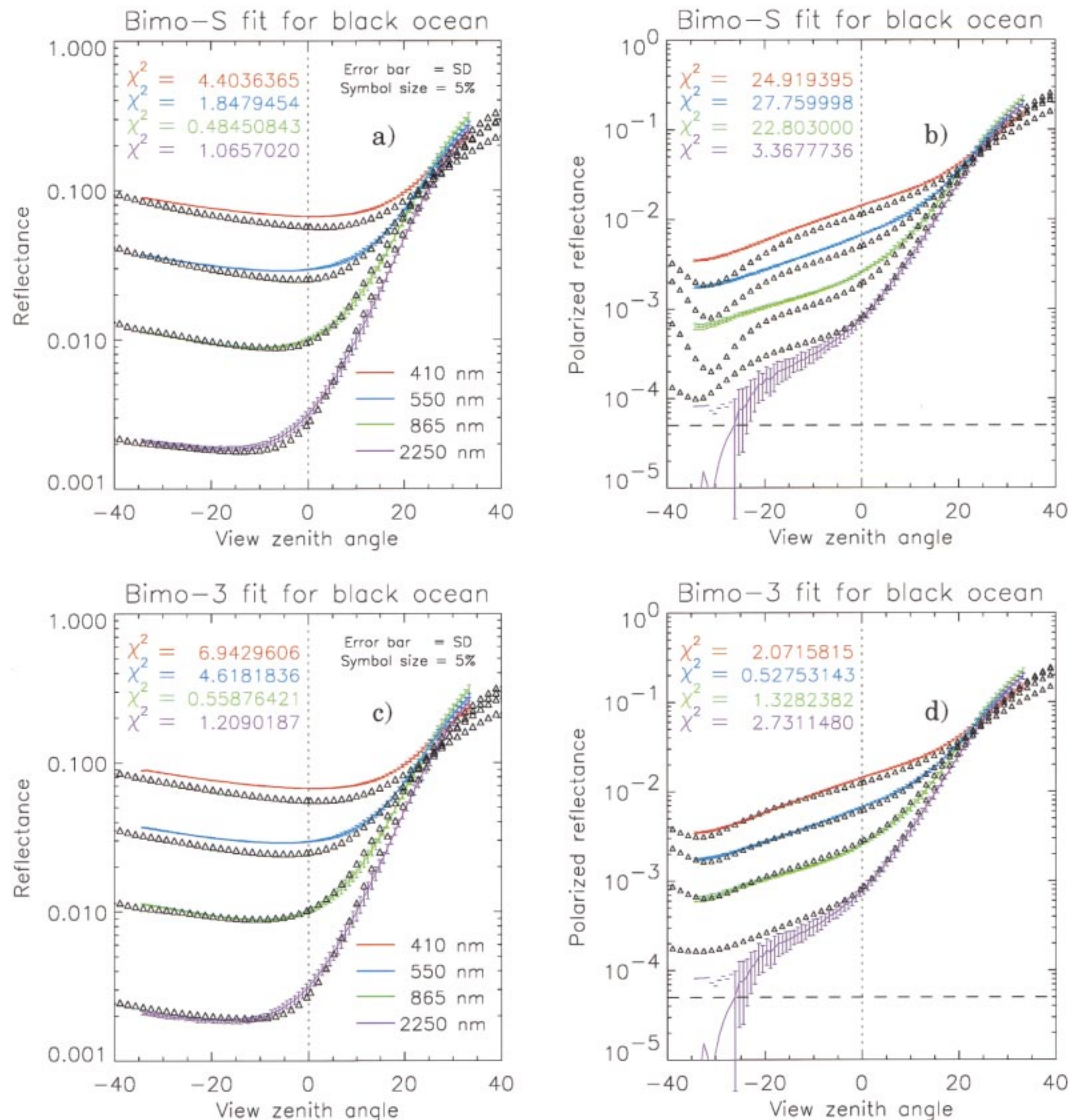


FIG. 6. (a) Lines and error bars show the mean RSP reflectance data and their std dev, respectively, for $\lambda = 0.410$, 0.550 , 0.865 , and $2.250 \mu\text{m}$ as in Fig. 4a. Symbols denote the corresponding fits using the bimo-S aerosol model specified in Table 3, and assuming a black ocean body. (b) Same as in (a) except for polarized reflectances. (c) Same as in (a) except for using the accumulation and coarse modes of the bimo-3 aerosol model listed in Table 2. (d) Same as in (c) except for polarized reflectances.

measurements. Thus, it is possible to retrieve an aerosol model and an ocean biophysical model that is consistent with all of the multispectral, multiangle polarized RSP measurements. Furthermore, comparing Figs. 5a and 5b shows that the polarized reflectance is a factor of 2 less sensitive to the contribution from underwater light scattering than the reflectance. Indeed, the difference between a purely molecular ocean (blue dashed line) and one with $[C] = 1 \text{ mg m}^{-3}$ (upper bound for most of the ocean; solid gray line) is now about equal to the uncertainty adopted for our simulations. The weak sensitivity of polarized reflectances to ocean color justifies their inclusion in our retrieval method, and shows the

potential of polarimetry to separate ocean color monitoring from atmospheric correction. We illustrate the estimation of an ocean biophysical model from measurements of this type by inverting the residual total reflectances to obtain the chlorophyll-like pigment concentration (C). The residual reflectances for our bimodal aerosol fit, shown in Fig. 5c, only become significant for measurements at wavelengths shorter than $0.670 \mu\text{m}$, which is spectrally consistent with case 1 water-leaving radiances (Gordon 1997). Approximating these radiances away from the sun glint by radiances originating from a Lambertian ocean leads to ocean body albedos of 0.0275 , 0.024 , and 0.0097 at 0.41 , 0.47 , and

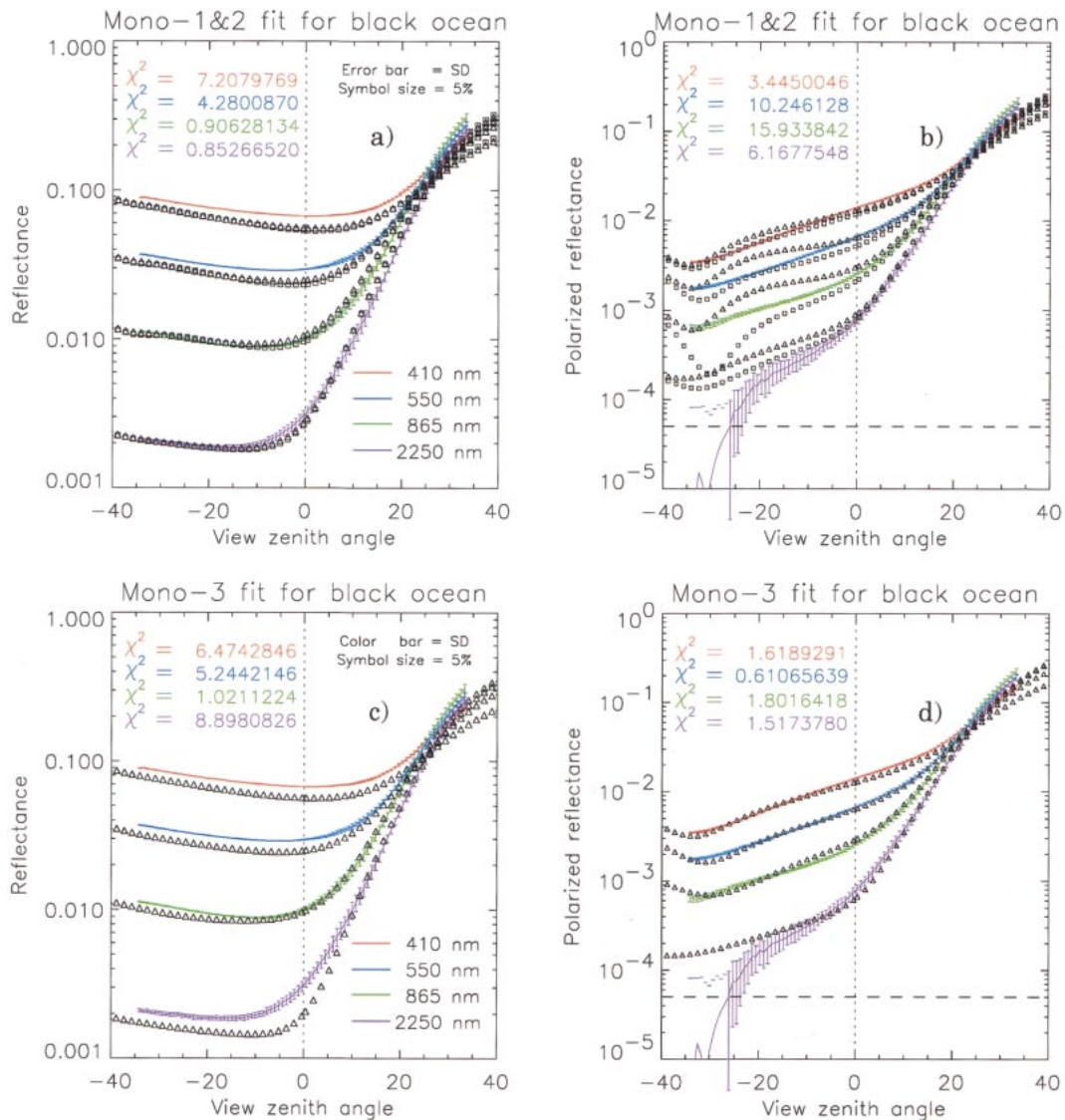


FIG. 7. (a) Lines and error bars show the mean RSP reflectance data and their std dev, respectively, for $\lambda = 0.410$, 0.550, 0.865, and 2.250 μm as in Fig. 4a. Triangles and boxes denote the corresponding fits using the mono-1 and mono-2 aerosol models listed in Table 2, respectively. The normalized chi-square values are given for the mono-1 fit. (b) Same as in (a), but for polarized reflectances. (c) Same as in (a), but for triangles denoting the fit using the mono-3 aerosol model listed in Table 2. (d) Same as in (c), but for polarized reflectances.

0.55 μm , respectively (Fig. 5d). The latter albedos are consistent with a chlorophyll-like pigment concentration $[C]$ of 0.30 mg m^{-3} based on the semiempirical curves shown in Fig. 5e (cf. Morel 1988), which is not unusual for this region of the ocean.

d. Aerosol retrieval using subsets of RSP data

We now examine how the accuracy of aerosol retrievals is affected by limiting the analysis to subsets of data. The rationale for this investigation is to examine what aspects of the multivariate aerosol model different measurement sets are sensitive to, with a view of under-

standing the types of discrepancies one might expect from retrievals using different satellite instruments. Figures 6a and 6b show the results of a bimodal aerosol fit that uses only the multiangle, multispectral total reflectance data subset. These measurements have a spectral range (0.41 to 2.25 μm) that is similar to the one monitored by MODIS. Their multiangle nature is also comparable to that of MISR data; that is, while their angular range is smaller they were obtained near the solar principal plane to maximize the range of scattering angles observed. Figure 6a shows that the observations at 0.865 and 2.25 μm can be well reproduced using the bimodal set of the water soluble and oceanic mix of the

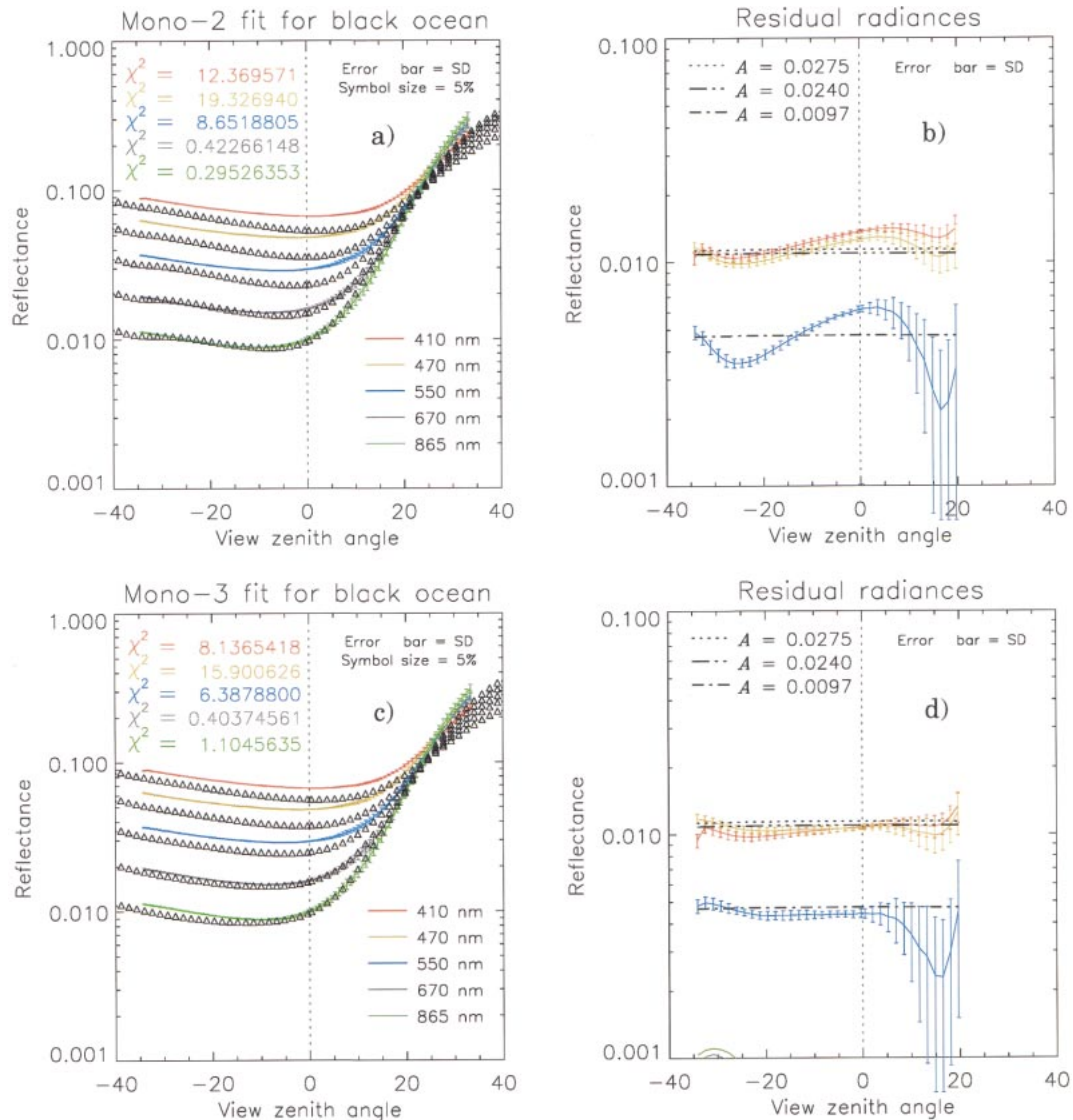


FIG. 8. (a) Lines and error bars show the mean RSP reflectance data and their std dev, respectively, for $\lambda = 0.410, 0.470, 0.550, 0.670,$ and $0.865 \mu\text{m}$ as in Fig. 5c. The symbols denote the corresponding fits using the mono-2 aerosol model listed in Table 2 and assuming a black ocean body. (b) Lines are for the same wavelengths as in (a) but denote the difference between the RSP data and corresponding fits. The black broken lines show the reflectances of water-leaving radiances simulated previously for the bimo-1 aerosol model case (cf. Fig. 5c). (c) Same as in (a), but for using the mono-3 aerosol model listed in Table 2. (d) Same as in (b), but for using the mono-3 aerosol model listed in Table 2

bimo-S aerosol model specified in Table 3. Note that these components are the same as those adopted by WMO (1986) except for (a) limiting the width of the oceanic aerosol size distribution to avoid incorporating unrealistically large “phantom” particles (Lacis and Mishchenko 1995), and (b) ignoring the strong absorption by the water soluble particles to compare with the results in section 4b. Predefined sets of aerosol candidate models such as these are commonly used for the inversion of photometric remote sensing data even though the temporal and spatial variability observed for tropospheric aerosols is much larger. This is because the information content provided by multiangle, multispec-

tral photometric remote sensing data is often insufficient to even partially resolve the multidimensional aerosol parameter space. Hence, the accuracy with which aerosols can be retrieved depends in these cases as much on the initial choice of aerosol candidate model as on the fit between measurements and simulations. Including polarization in the remote sensing of aerosols reduces the nonuniqueness of the inversion problem because the measurements are sensitive to refractive index and allow for the discrimination and quantification of two modes of the aerosol size distribution (see Fig. 6b). For example, the presence of the WMO (1986) water-soluble (oceanic) aerosol particles causes the polarized

reflectance to decrease much more (less) than observed by the RSP instrument for $\theta \approx -32^\circ$ and $\lambda = 0.865 \mu\text{m}$ ($\lambda = 2.25 \mu\text{m}$). In Figs. 6c and 6d we consider the results of a bimodal aerosol retrieval based on the inversion of multiangle photo-polarimetric measurements obtained at $\lambda \leq 0.865 \mu\text{m}$, that is, of observations that have the same spectral range as those obtained by the POLDER instrument. There are three features of our analysis of this data subset that should be emphasized. First, no solutions could be found using the water-soluble and/or oceanic aerosol models of Table 3 as substitutes for the accumulation and/or coarse mode aerosol in our retrieval algorithm. Second, the accumulation mode component of the retrieved bimodal aerosol resembled that of bimo-1 in Table 2, which is consistent with our discussion of Figs. 4c and 4d. Third, the 0.865- and 0.55- μm polarized reflectance measurements remained sensitive enough to large particles to rule out many coarse-mode aerosol models. Such results are encouraging, suggesting that the use of polarimetry remains a powerful remote sensing tool even for small spectral ranges. Nevertheless, the absence of 2.25- μm measurements leads to the retrieval of a bimodal aerosol (hereafter referred to as bimo-3) whose coarse-mode particles are smaller and have a smaller refractive index than those of the initial retrieval using all the RSP data (cf. bimo-1 in Table 2). This is because the 2.25- μm measurements are essentially insensitive to accumulation mode aerosols but provide much of the sensitivity to coarse mode aerosols.

An alternative to the bimodal aerosol candidate models examined above, is to use monomodal aerosol models when analyzing subsets of RSP-like data. This approach is less time consuming since the dimensionality of the parameter space has been reduced and the non-uniqueness problems discussed above are buried in the a priori assumption about the functional form of the aerosol size distribution. Nonetheless, if such distributions provide acceptable results their simplicity is a desirable feature in the estimation problem which constitutes an aerosol retrieval. A monomodal model is not however acceptable for the analysis of the complete RSP dataset and so no monomodal inversion on the complete RSP dataset is presented. Figures 7a and 7b show the results of such a retrieval using only the multiangle, multispectral total reflectance data. In Fig. 7a it can be seen that the observations at 0.865 and 2.25 μm (solid lines) are now consistent with two different monomodal aerosol models (symbols). These two microphysical models, henceforth denoted mono-1 (triangles) and mono-2 (boxes), have the same effective radius (0.4 μm), but differ significantly in refractive index (0.06, see Table 2). The polarized reflectance measurements (Fig. 7b) are completely inconsistent with these two microphysical models, ruling them out as acceptable solutions to the aerosol retrieval problem. This further demonstrates the sensitivity of polarization measurements to the particle refractive index as compared to

reflectance measurements. Once again we observe that a radiance-only dataset can lead to the retrieval of aerosol models that are significantly in error without any indication from the data itself that this is the case. In Figs. 7c and 7d we consider the results of a monomodal aerosol retrieval for a dataset of multiangle photo-polarimetric measurements obtained at $\lambda \leq 0.865 \mu\text{m}$. The relatively large optical thickness of accumulation-mode particles still allows for an acceptable retrieval using a monomodal aerosol model (hereafter denoted by mono-3) with a refractive index and size distribution close to those of the accumulation-mode component of bimo-1, which was our original retrieval (Table 2). Note also that while the mono-3 aerosol optical thickness is significantly larger (34%) than that of the bimo-1 accumulation-mode aerosol at 0.55 μm , its column particle number density (N) is only slightly larger (5%) than that of the bimo-1 accumulation-mode aerosol. Mishchenko et al. (1997b) found that it is much more difficult to determine N than to retrieve the optical depth for accumulation-mode particles, based on single-channel sensitivity analyses. The mono-3 aerosol retrieval results suggests that this problem may well be reduced by including multispectral, multiangle measurements of intensity and polarization in the inversion process.

For the sake of completeness, we show in Fig. 8 the water-leaving residual reflectances based on aerosol retrievals assuming a monomodal aerosol size distribution, as described above. The results for the mono-2 aerosol model are given in Fig. 8a, where it is apparent that the atmospheric correction using intensity-only measurements and an assumed monomodal size distribution (based on the model shown in Fig. 7a) leads to significant errors in the bidirectional behavior of the ocean-body reflectance (Fig. 8b). The residual water-leaving reflectances for the mono-3 aerosol model are shown in Fig. 8c. The bidirectional behavior of the ocean-body reflectance that is inferred for this case (Fig. 8d) is similar to the results shown in Fig. 5d. The fact that the atmospheric correction using POLDER-like measurements yields better results for the ocean-body analyses than reflectance-only measurements is provocative, but any definitive conclusions about the relative superiority of these two types of measurement will require a more detailed and complete analysis.

5. Conclusions

An analysis of data obtained over the ocean by an airborne version of EOSP, the Research Scanning Polarimeter (RSP), shows that bimodal size information, composition (via refractive index), aerosol optical depth, and number density can be retrieved from multispectral, multiangle polarization measurements. The aerosol optical depth retrieved from the RSP data is consistent with sun photometer measurements (difference of 0.008 at 0.55 μm). The weak sensitivity of polarized reflectances at shorter wavelengths (0.41 and

0.55 μm) to ocean color allows for their inclusion in the retrieval of aerosol properties and shows the potential of polarimetry to separate ocean color monitoring from atmospheric correction. We note that analyses of reflectance-only data subsets are not capable of distinguishing monomodal from bimodal aerosol solutions, nor do they provide strong constraints on aerosol refractive indices. The errors in aerosol retrievals from these reflectance-only data subsets are seen to propagate into errors in the estimated ocean color. The simulated examples of POLDER retrievals indicates useful sensitivity to the refractive index, size, and optical depth of the accumulation-mode aerosol, but the absence of longer wavelength (2.25 μm) measurements limits the amount of information that can be obtained about the coarse-mode aerosol. Since the errors in the estimated accumulation mode are small, the estimate of ocean color from the POLDER-like data subset is similar to that obtained from the complete dataset, suggesting that the inclusion of polarized reflectances from the shorter wavelength bands of POLDER may be useful in improving aerosol retrievals from this type of data.

The accurate polarimetric measurements made by the RSP, over a broad angular and spectral range, significantly reduce the nonuniqueness problem in the retrieval of aerosol properties by providing information about the spectral refractive index and both accumulation and coarse-mode size distribution parameters. This capability allows aerosol parameters to be determined with the accuracy needed for long-term monitoring of the direct and indirect aerosol forcings of climate. The analysis of polarized reflectances at shorter wavelengths (0.41 and 0.55 μm) indicates the potential of these measurements to further improve aerosol retrievals and atmospheric correction for ocean color monitoring.

Acknowledgments. This research was funded in part by NASA through the EOS and GACP programs and by the Department of Energy Interagency Agreement under the Atmospheric Radiation Measurement program. The provision of sun-photometer data from an instrument in the Solar Irradiance Research Network (SIRN) by Dr. Barbara Carlson of NASA GISS is gratefully acknowledged. The authors would also like to thank Dr. Johan de Haan and an anonymous reviewer for their insightful and helpful comments, which improved the final version of this manuscript.

REFERENCES

- Alexandrov, M. D., A. A. Lacis, B. E. Carlson, and B. Cairns, 2002: Remote sensing of atmospheric aerosols and trace gases by means of Multifilter Rotating Shadowband Radiometer. Part I: Retrieval algorithm. *J. Atmos. Sci.*, **59**, 525–544.
- Bréon, F.-M., and P. Goloub, 1998: Cloud droplet effective radius from space-borne polarization measurements. *Geophys. Res. Lett.*, **25**, 1879–1882.
- Cairns, B., L. D. Travis, and E. E. Russell, 1999: The Research Scanning Polarimeter: Calibration and ground-based measurements. *Polarization: Measurements, Analysis, and Remote Sensing II*, D. H. Goldstein and D. B. Chenault, Eds., *Proc. SPIE*, Vol. 3754, 186–196.
- Chowdhary, J., 1999: Multiple scattering of polarized light in atmosphere-ocean systems. Application to sensitivity analyses of aerosol polarimetry, Ph.D. thesis, Columbia University, 280 pp.
- , B. Cairns, M. Mishchenko, and L. Travis, 2001: Retrieval of aerosol properties over the ocean using multispectral and multi-angle photopolarimetric measurements from the Research Scanning Polarimeter. *Geophys. Res. Lett.*, **28**, 243–246.
- Chylek, P., G. Videen, D. J. W. Geldart, J. S. Dobbie, and H. C. W. Tso, 2000: Effective medium approximations for heterogeneous particles. *Light Scattering by Nonspherical Particles: Theory, Measurements, and Applications*, M. I. Mishchenko et al., Eds., Academic Press, 273–308.
- Cox, C., and W. Munk, 1954: Statistics of the sea-surface derived from sun-glitter. *J. Mar. Res.*, **13**, 198–227.
- d’Almeida, G. A., P. Koepke, and E. P. Shettle, 1991: *Atmospheric Aerosols: Global Climatology and Radiative Characteristics*. Deepak Publishing, 561 pp.
- De Haan, J. F., P. B. Bosma, and J. W. Hovenier, 1987: The adding method for multiple scattering calculations of polarized light. *Astron. Astrophys.*, **183**, 371–391.
- Dentener, F. J., and P. Crutzen, 1993: Reaction of N_2O_5 on tropospheric aerosols: Impact on the global distributions of NO_x , O_3 , and OH. *J. Geophys. Res.*, **98**, 7149–7163.
- Deuzé, J. L., P. Goloub, M. Herman, A. Marchand, G. Perry, S. Susana, and D. Tanré, 2000: Estimate of the aerosol properties over the ocean with POLDER. *J. Geophys. Res.*, **105**, 15 329–15 346.
- Diner, D. J., and Coauthors, 1991: A Multi-angle Imaging SpectroRadiometer for terrestrial remote sensing from the Earth Observing System. *Int. J. Imaging Syst. Technol.*, **3**, 92–107.
- Dubovik, O., and M. D. King, 2000: A flexible inversion algorithm for retrieval of aerosol optical properties from Sun and sky radiance measurements. *J. Geophys. Res.*, **105**, 20 673–20 696.
- Frouin, R., M. Schindling, and P.-Y. Deschamps, 1996: Spectral reflectance of sea-foam in the visible and near-infrared: In-situ measurements and remote sensing applications. *J. Geophys. Res.*, **101**, 14 361–14 371.
- Goloub, P., D. Tanré, J. L. Deuzé, M. Herman, A. Marchand, and F.-M. Bréon, 1999: validation of the first algorithm applied for deriving aerosol properties over the ocean using the POLDER/ADEOS measurements. *IEEE Trans. Geosci. Remote Sens.*, **37**, 1586–1596.
- Gordon, H. R., 1997: Atmospheric correction of ocean color imagery in the Earth Observing System era. *J. Geophys. Res.*, **102**, 17 081–17 106.
- , and A. Y. Morel, 1983: *Remote Assessments of Ocean Color for Interpretation of Satellite Visible Imagery: A Review*. Springer-Verlag, 114 pp.
- Hale, G. M., and M. R. Querry, 1973: Optical constants of water in the 200-nm to 200- μm wavelength region. *Appl. Opt.*, **12**, 555–563.
- Hansen, J. E., and L. D. Travis, 1974: Light scattering in planetary atmospheres. *Space Sci. Rev.*, **16**, 527–610.
- , and Coauthors, 1995: Low-cost long term monitoring of global climate forcings and feedbacks. *Climatic Change*, **31**, 247–271.
- Higurashi, A., and T. Nakajima, 1999: Development of a two channel aerosol retrieval algorithm on a global scale using NOAA/AVHRR. *J. Atmos. Sci.*, **56**, 924–941.
- Houghton, J. T., L. G. Meira Filho, B. A. Callender, N. Harris, A. Kattenberg, and K. Maskell, Eds., 1996, *Climate Change 1995: The Science of Climate Change*. Cambridge University Press, 572 pp.
- Jaenicke, R., 1993, Tropospheric aerosols. *Aerosol-Cloud-Climate Interactions*, P. V. Hobbs, Ed., Academic Press, 1–30.
- Kadyshevich, Y. A., and Y. S. Lyubovtseva, 1973: Certain characteristics of ocean hydrosols from scattering matrices. *Izv. Acad. Sci. USSR Atmos. Oceanic Phys.*, **9**, 659–663.

- King, M. D., and B. M. Herman, 1979: Determination of the ground albedo and index of absorption of atmospheric particulates by remote sensing. Part I: Theory. *J. Atmos. Sci.*, **36**, 163–173.
- , Y. J. Kaufman, W. P. Menzel, and D. Tanré, 1992: Remote sensing of cloud, aerosol, and water vapor properties from the MODerate Imaging Spectroradiometer. *IEEE Trans. Geosci. Remote Sens.*, **30**, 2–27.
- Koepke, P., 1984: Effective reflectance of oceanic whitecaps. *Appl. Opt.*, **23**, 1816–1842.
- Lacis, A. A., and M. I. Mishchenko, 1995: Climate forcing, climate sensitivity, and climate response: A radiative modeling perspective on atmospheric aerosols. *Aerosol Forcing of Climate*, R. J. Charlson and J. Heintzenberg Eds., Wiley, 11–42.
- Loisel, H., and A. Morel, 1998: Light scattering and chlorophyll-concentration in case 1 waters: A reexamination. *Limnol. Oceanogr.*, **43**, 847–858.
- Masuda, K., 1988, Effects of the speed and direction of surface winds on the radiation in the atmosphere–ocean system. *Remote Sens. Environ.*, **64**, 53–63.
- Mishchenko, M. I., and L. D. Travis, 1997a: Satellite retrieval of aerosol properties over the ocean using polarization as well as intensity of reflected sunlight. *J. Geophys. Res.*, **102**, 16 989–17 013.
- , and —, 1997b: Satellite retrieval of aerosol properties over ocean using measurements of reflected sunlight: Effect of instrumental errors and aerosol absorption. *J. Geophys. Res.*, **102**, 13 543–13 553.
- , —, R. A. Kahn, and R. A. West, 1997a: Modeling phase functions for dustlike tropospheric aerosols using a shape mixture of randomly oriented polydisperse spheroids. *J. Geophys. Res.*, **102**, 16 831–16 847.
- , —, W. B. Rossow, B. Cairns, B. E. Carlson, and Q. Han, 1997b: Retrieving CNN column density from single-channel measurements of reflected sunlight over the ocean: A sensitivity study. *Geophys. Res. Lett.*, **24**, 2655–2658.
- , I. V. Geogdzhayev, B. Cairns, W. B. Rossow, and A. A. Lacis, 1999: Aerosol retrievals over the ocean by use of channels 1 and 2 AVHRR data: Sensitivity analysis and preliminary results. *Appl. Opt.*, **38**, 7325–7341.
- Mobley, C. D., and Coauthors, 1993: Comparison of numerical methods for computing underwater light. *Appl. Opt.*, **32**, 7484–7504.
- Monahan, E. C., and I. G. O’Muircheartaigh, 1980: Optical power law description of oceanic whitecap coverage dependence on windspeed. *J. Phys. Oceanogr.*, **10**, 2094–2099.
- Morel, A., 1974: Optical properties of pure water and pure sea water. *Optical Aspects of Oceanography*, N. G. Jerlov and E. Steeman Nielsen, Eds., Academic Press, 1–24.
- , 1988: Optical modeling of the upper ocean in relation to its biogenic matter content (Case I: Waters). *J. Geophys. Res.*, **93**, 10 749–10 768.
- , and B. Gentili, 1995, Diffuse reflectance of oceanic waters. II. Implication of bidirectionality for the remote sensing problem. *Appl. Opt.*, **35**, 4850–4862.
- Nakajima, T., G. Tonna, R. Rao, P. Boi, Y. Kaufman, and B. Holben, 1996: Use of the sky brightness measurements from the ground for remote sensing of particulate polydispersions. *Appl. Opt.*, **35**, 2672–2696.
- Noxon, J. F., 1978: Tropospheric NO₂. *J. Geophys. Res.*, **83**, 3051–3057.
- Petzold, T. J., 1977: Volume scattering functions for selected ocean waters. *Light in the Sea*, J. E. Tyler, Ed., Dowden, Hutchinson and Ross, 152–157.
- Pujadas, M., J. Plaza, J. Teres, B. Artinano, and M. Millan, 2000: Passive remote sensing of nitrogen dioxide as a tool for tracking air pollution in urban areas: The Madrid urban plume, a case of study. *Atmos. Environ.*, **34**, 3041–3056.
- Sancer, M. I., 1969: Shadow-corrected electromagnetic scattering from a randomly-rough ocean surface. *IEEE Trans. Antennas Propagation*, **17**, 557–585.
- Shaw, G. E., 1976: Nitrogen dioxide—Optical absorption in the visible. *J. Geophys. Res.*, **81**, 5791–5792.
- Stowe, L. L., and A. M. Ignatov, 1997: Development, validation, and potential enhancements to the second-generation operational aerosol product at the National Environmental Satellite, Data, and Information Service of the National Oceanic and Atmospheric Administration. *J. Geophys. Res.*, **102**, 16 923–16 934.
- Stramski, D., and D. A. Kiefer, 1991: Light scattering by microorganisms in the open ocean. *Progress in Oceanography*, Vol. 28, Pergamon Press, 343–383.
- Tanré, D., M. Herman, and Y. J. Kaufman, 1996: Information on aerosol size distribution contained in solar reflected spectral radiances. *J. Geophys. Res.*, **101**, 19 043–19 060.
- Toole, D. A., D. A. Siegel, D. W. Menzies, M. J. Neumann, and R. C. Smith, 2000: Remote-sensing reflectance determinations in the coastal ocean environment: Impact of instrumental characteristics and environmental variability. *Appl. Opt.*, **39**, 456–469.
- Travis, L. D., 1993: Earth Observing Scanning Polarimeter. *Long-Term Monitoring of Global Climate Forcing and Feedbacks*, J. Hansen et al., Eds., NASA Conf. Publ. 3234, 40–46.
- Volten, H., and Coauthors, 1998: Laboratory measurements of angular distributions of light scattered by phytoplankton and silt. *Limnol. Oceanogr.*, **46**, 1180–1197.
- Voss, K. J., and E. S., Fry, 1984: Measurements of the Mueller matrix for ocean water. *Appl. Opt.*, **23**, 4427–4439.
- WMO, 1986: A preliminary cloudless standard atmosphere for radiation computation. Radiation Commission Tech. Rep. WCP-112, WMO/TD-No. 24, 53 pp.